International Journal of Hydrogen Energy 54 (2024) 1273–1285

Contents lists available at ScienceDirect

International Journal of Hydrogen Energy

journal homepage: www.elsevier.com/locate/he

# Design, development, integration and evaluation of hybrid fuel cell power systems for an unmanned water surface vehicle

Jordi Renau [a,*], Diego Tejada [b], Víctor García [a], Eduardo López [b], Luis Domenech [a], Antonio Lozano [c], Félix Barreras [c]

[a] Cardenal Herrera University, CEU Universities, C/ San Bartolomé 55, Alfara del Patriarca, 46115, Valencia, Spain
[b] Instituto Nacional de Técnica Aerospacial (INTA), Área de Energía y Medio Ambiente - Laboratorio de Energía de El Arenosillo, Ctra. S. Juan-Matalascañas, km34, Mazagón, 21130, Huelva, Spain
[c] Instituto de Carboquímica, CSIC, Miguel Luesma Castán, 4, Zaragoza, 50018, Zaragoza, Spain

ARTICLE INFO

*Keywords:*
Ion-Li battery
Hydrogen
PEM fuel cell
USV
Hybrid power plants

ABSTRACT

When fuel cells are used to power mobile applications, such a vehicles, hybridization with batteries is normally required. Depending on the electronic coupling between the energy sources the power plants can have passive or active configurations. Hybrid fuel cell-battery power plants with active power control flow have some advantages. For example, they can decrease the total energy losses, while improving the fuel cell performance, extending its lifetime. Power plants with DC/DC converters show low specific energy ratios, but with a superior energy management. In the present research, the hybrid power plant for an unmanned aquatic surface vehicle (USV) based on a PEM fuel cell and a Li-ion battery is developed. Active (with DC–DC converters) or passive architectures are analyzed by numerical simulations and experimental tests. Good results are obtained for the active power plant, where the peak power demands are managed by the battery pack while the fuel cell power remains constant thanks to the DC-converter control. The study shows that a simple control algorithm (no optimal) can help to extend the USV autonomy above 12 h in calm waters with a specific energy of 85.6 W h kg$^{-1}$.

## 1. Introduction and background

In recent years, there has been a growing demand for unmanned vehicles in multiple domains, spurred by tasks that are inherently repetitive, unpleasant and/or dangerous to human operators. This is partly due to their capabilities to provide high quality data in a safe way at lower cost than other traditional methods. Despite these advantages, the limited endurance and operational time achieved by such systems, in particular in electric vehicles, are barriers to their potential development in new applications. On-board energy storage is one of the most relevant issues in the design, development and operation of these platforms, taking into account its direct impact on their endurance and, consequently, overall performance.

Nowadays, the electric propulsion is predominant in small size unmanned vehicles (aerial, ground and marine platforms), and the only feasible solution in some cases, as in unmanned submarines. Usually, their energy storage systems are based on lead–acid or lithium-ion batteries. Despite the rapid progress of these technologies, there are still some gaps to overcome in the electric power systems [1]. A feasible approach is to combine multiple energy storage/conversion technologies on the same power plant. A solution particularly attractive is the integration of fuel cells and batteries in hybrid configurations, which have been successfully tested and evaluated in mobile applications [2–11]. Hybridization of vehicle power plants is a clear improvement in terms of cost, energy efficiency and it is a necessity for fuel cells technology [12,13]. Fuel cell stacks need to use an additional energy storage system, like a battery or a supercapacitor, due to its slow power demand response [14], its sensitivity to load variations, that influences its longevity and its difficulty to cold start [15,16]. Fuel cells electric vehicles are like pure battery electric ones but with extended ranges and faster refueling times [12,17]. Nevertheless, the hydrogen infrastructure is years after the electrical recharging posts.

This paper presents the development of an aquatic unmanned surface vehicle and its hybrid fuel cell-battery power plant. The development is under the frame of the project: “Optimal design and integration of polymer electrolyte membrane (PEM) fuel cell-based flexible hybrid powerplants for autonomous and remotely piloted electric vehicles (DOVELAR)”. The power system is based on the coupling of a PEM fuel cell and Li-ion batteries, either directly or through DC/DC converters. Both possible configurations have been simulated and the active power plant tested in a laboratory bench.

* Corresponding author.
*E-mail address:* jordi.renau@uchceu.es (J. Renau).

https://doi.org/10.1016/j.ijhydene.2023.12.043
Received 15 June 2023; Received in revised form 30 November 2023; Accepted 4 December 2023
Available online 8 December 2023

**Table 1**
Dovelar USV main specifications.

| DOVELAR USV | |
|---|---|
| Dimensions (L × W × H) | (102 × 63 × 22) cm |
| Draft | 12 cm |
| Weight | 12 kg |
| Hull material | ABS + Carbon fiber reinforced |
| Propulsion | 250 W DC brushless motor |
| Endurance[a] | 12 h at 2 kn (≈1 m s$^{-1}$) |

[a] Target value, based on the hybrid PEM fuel cell + Li-ion battery powerplant.

The outline of the paper can be summarized as follows. In Section 2 the vehicle and the power plant are described. Section 3 outline the development of the power plant and the characterization of the elements. Section 4 describe and analyze the result from the simulation of the power plant using software open source Modelica. In Section 5 experimental results are shown and discussed. Finally, Section 6 summarize the main conclusions and outlines the future work.

## 2. Description of the experimental unmanned platform

The Unmanned Aquatic Surface Vehicle (USV) platform is composed of two separate general parts. Firstly, the vehicle hull, which includes the propulsion and motorization. And secondly, the vehicle power plant. Both components had been entirely designed and developed by the research team.

The USV platform is a prototype designed in the frame of a coordinated research project with researchers from four institutions: "Instituto de Carboquímica" (ICB-CSIC),. "Universidad Politécnica de Cataluña" (UPC), the "National Institute of Aerospace Technology" (INTA) and the "Cardenal Herrera University CEU" (UCHCEU).

The USV is an unmanned surface vehicle that can be both, autonomous or remotely piloted depending on the mission and targets. The vehicle uses an embedded computer with a Robot Operating System (ROS) that controls both the throttle and the rudder. ROS integrates the navigation, positioning and collision-avoidance systems, all in one. The embedded computer also acts as a telemetry system within radio communication. The power plant is controlled independently using an electronic board designed and manufactured by the research group based on an Arduino Mega microcontroller. The electronic board and the ROS system communicate using a USB serial transfer protocol, developed for this purpose. ROS provides the position and acceleration orders to the vehicle from the navigation algorithm, and the Arduino microcontroller feeds the ROS telemetry with the power plant data, namely, fuel cell parameters, battery state of charge and hydrogen reserve. The power plant is further described in Section 2.2.

### 2.1. Design and manufacture of the vehicle hull

For the design of the USV a three-phase approach methodology was used. In the first phase, an initial geometry was defined trying to maximize the compliance with all the operational and manufacturing requirements imposed on the prototype, Then, the main design was validated and adjusted through CFD analysis. Finally, in the third phase, the manufactured prototype was experimentally validated in the "El Pardo Center for Hydrodynamic Experiences" (INTA–CEHIPAR) towing tank facility.

The proposed USV platform has been designed to operate at low speed (≈1 m s$^{-1}$) in shallow fresh water reservoirs and lakes, especially for monitoring tasks in wetlands, integrating scientific sensors and equipment for measure physical, chemical and biological parameters in these locations. The photo in Fig. 1 depicts the finished hull, including the fuel cell during the assembly process after all the design and experimental validations. Main specifications of the USV are summarized in Table 1.

Fig. 2(a) shows the USV under experimentation in the CEHIPAR calm water towing tank, where the final hull design was validated and the drag power was estimated. The results for the propulsion resistance are depicted in Fig. 2(b), from 0.6 to 1.4 m s$^{-1}$. As can be observed the drag power for the designed velocity is around 7.5 W. This value only reflects the power needed to keep the hull at the constant rated speed, but efficiency and payload consumptions have to be added to establish the total required power. Ancillary total installed power achieves the value of 213 W. This estimation was done adding the rated power of all the installed devices, which are the fans for control temperature, all the sensoring and the navigation embedded computer (ROS). However the measured total simultaneous power consumption was around 83 W. Concluding that the USV will need 120 W considering the drag the payload consumptions and adding a security factor of 30% just to improve the manoeuvrability of the USV, in case it should be required.

### 2.2. Power plant electrical architecture

The power plant is the main energy source for the USV propulsion and ancillary systems. The power system is a hybrid fuel cell-battery configuration and the final solution for the USV is being evaluated between two different architectures considered as function of the power electronic coupling between energy sources: a passive and an active power plant [18,19].

The passive configuration (left image in Fig. 3) implies the direct coupling between fuel cells and batteries in a common DC bus. A power diode is what defines the configuration as a "passive" architecture. The diode location can be either sources, in the fuel cell or in the battery output. The objective of the diode is not only to protect against overvoltage and -current, but also to control the energy flows. The diode after the fuel cell sets the battery as the main source and allows the battery recharging from the hydrogen during low-energy demand. The system is configured as a range-extended power plant [7,20]. This is the considered passive architecture for the USV. On the other hand, when the diode is directly connected to the battery, it acts as a power booster, giving support to the hydrogen fuel cell in case of high power demand. This would be a preferable configuration for unmanned aerial vehicles [14]. Passive configuration provides lower losses, reduced cost and a simpler architecture control than an active counterpart. However, the capability to optimize the operating point of the main components is limited. Furthermore, if this option is considered, a careful design and integration of the fuel cell and batteries is required to ensure a similar voltage range operation and proper charging conditions of the batteries from the fuel cell.

In an active power plant architecture, a decoupling of the sizing and operating conditions between batteries and fuel cell is possible thanks to the DC/DC converters. A better control of the power system is also possible. Right image in Fig. 3 shows the electrical connection of an active hybrid power system. The main disadvantages of active configurations are the more complex system topology, a lower efficiency due to voltage losses, a higher system cost, and higher weight and volume [5]. As in the case of the diode, the power electronic converter can be installed either in the fuel cell or in the battery output, but the best option is to have it controlling the fuel cell system, because it is more expensive and delicate.

The preliminary characterization of both topologies involves the same fuel cell and batteries, although the active configuration would allow more flexibility regarding fuel cell specifications. In both cases, a suitable Energy Management System (EMS) has been specifically designed and developed, which is responsible for the overall monitoring and control of the fuel cell system, batteries and DC/DC converter in the active configuration. In both cases, the voltage of the DC bus will depend on the load operating requirements, and the battery state of charge.

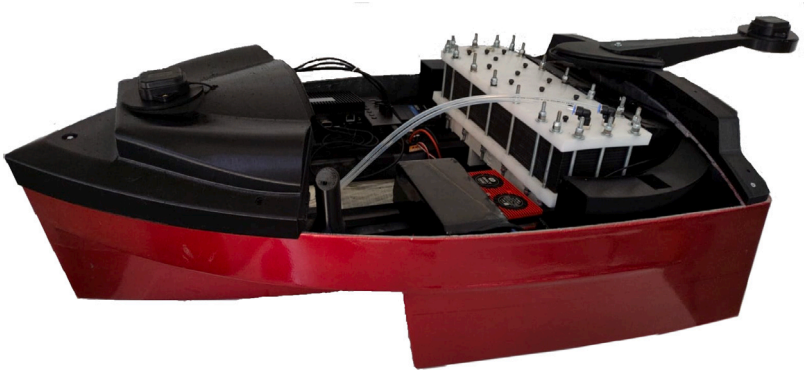

**Fig. 1.** USV integration process, where the fuel cell and the battery are installed.

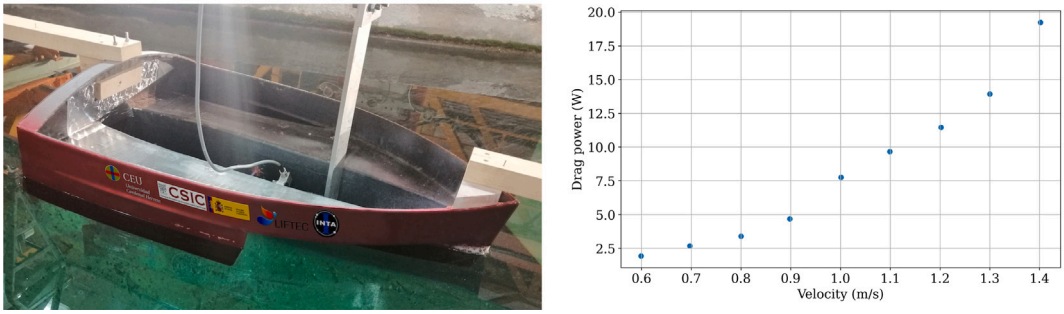


(a) USV in the test tank (b) CEHIPAR results

**Fig. 2.** Calm water towing tank in CEHIPAR-INTA facilities.

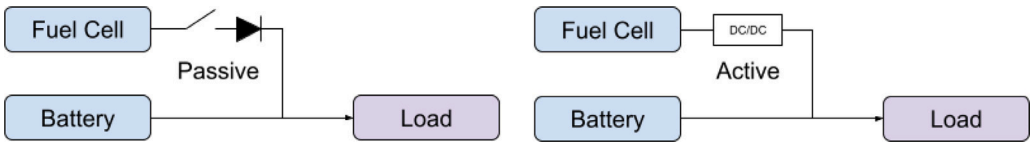


**Fig. 3.** Active and passive powerplant circuit diagram.

### 2.3. Fuel cell and hydrogen system

The hybrid power system integrates a 500 W open cathode PEM fuel cell, designed and developed in the framework of this project (Fig. 4). The stack consists of 15 cells with and active area of 200 $cm^2$ and it has been designed to provide a nominal electric power of 500 W at 70 A. Bipolar plates have been manufactured in JP-945 graphite [21], with parallel channel flowfield geometries have been used in both sides. In this configuration, the air stream is propelled throughout the cathode channels by axial fans both to ensure the amount of oxygen needed for the cathodic reaction, and to keep the stack temperature in the suitable range specified by the MEA manufacturer (below 40 °C), removing the excess heat by forced convection.

Anode sides include 38 channels, with a depth of 1.2 mm and 1 mm wide, while the cathode geometry is formed by 70 channels with a width of 3 mm and a depth of 2 mm form the geometry for the cathode side. This represents 63% of the plate area open to air flow, with the remaining 37% for electric contact between GDL and ribs. The gas distribution manifolds (inlet and outlet) are rectangular ducts 80 mm long and 10 mm wide that ensure a homogeneous gas distribution to each cell of the stack. The selected cooling system selected includes two fans assembled in parallel configuration as depicted in Fig. 4(b). Cooling system is integrated into the hull design to provide also interior ventilation.

#### 2.3.1. Hydrogen storage system

The hydrogen storage system is based on compressed gas, which is a mature and commercially available technology (Fig. 5). It can offer a more suitable performance in terms of specific energy and refueling time than metal hydrides, the other option considered. This storage system comprises a Type III pressure cylinder, with a weight of 2.8 kg, an internal volume of 4.7 L and a service pressure of 300 bar. Assuming a 37%[1] fuel cell efficiency and hydrogen compressibility (24 kg $m^{-3}$), it can store a total energy around 1670 W h, large enough to achieve the target operation of 12 h, improved if the energy stored in the batteries is added. The fuel cell hydrogen system has an specific energy of 118 W h $kg^{-1}$.

Another critical component of the system is the pressure regulator, because its weight and size can significantly affect the specific energy density target. In this case, a light-weight two-step pressure regulator has been selected. Suitable temperature and pressure sensors have also been assembled to monitor the safe operation and performance of the system, in both states when discharging and when refueling hydrogen to the tank.

[1] Considering the HHV of the hydrogen and a fuel consumption efficiency of 95%.

(a) Cathode air channels point of view (b) Cooling system

**Fig. 4.** Assembled stack with the air cooling system installed.

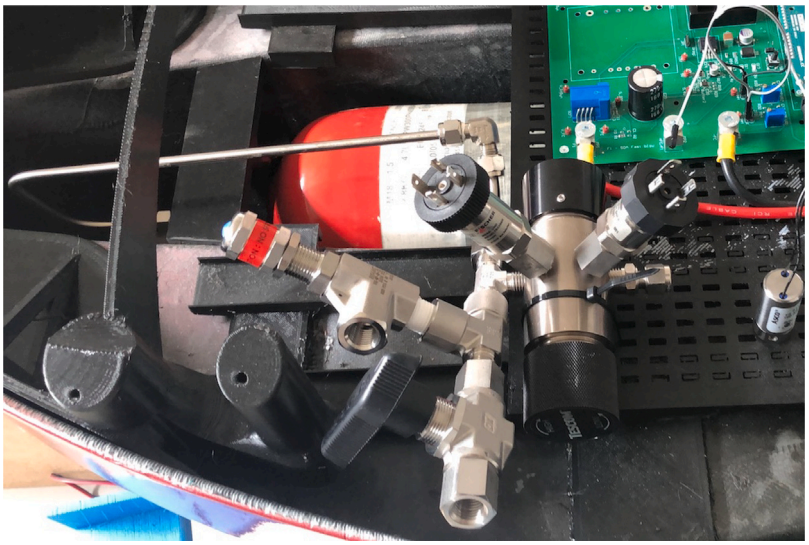

**Fig. 5.** Storage system assembled in the USV.

**Fig. 6.** Comparative of both DC converters used, ad-hoc DC–DC converter (left) and commercial converter (right), both for up to 1 kW.

### 2.4. Battery energy storage system

The battery energy storage system is based on assembled LiPo cells connected in series and parallel. The number of cells in series will define the rated voltage of the battery, which is a design parameter that is important for the power plant performance and critical for the passive strategy architecture.

Battery packs are assembled all with the same LiPo cells of 23 A h nominal capacity (C), with and specific energy of 173 W h $kg^{-1}$ per cell (472.5 g per cell with wiring). Each cell has a maximum charge current of 115 A (5C), a maximum discharge current of 230 A (10C), and a peak discharge current of 345 A (15C). The expected life-time for these cells is estimated to be higher than 500 cycles, depending on the charging/discharging conditions. In this way, to avoid deep discharge, the minimum voltage per cell when integrated in the hybrid power system will be 3 V, with a maximum of 4.2 V per cell. Temperature is also a critical issue for LiPo batteries, 0–45 °C being the recommended operating range for these cells.

## 3. Development of hybrid fuel cell-battery power plant

The fuel cell and the battery (cells and packs) have been preliminary characterized to evaluate their main performance in terms of current, voltage and power. In the case of the batteries, the packs have been tested according to charging/discharging cycles at different C-rates. The two different power plant architectures considered require the use of two different battery packs due to voltage compatibility. In the case of the passive architecture only a battery pack of two cells in series (2S) can be used due to the fuel cell rated voltage to ensure

**Table 2**
Operative conditions for passive strategy at the fuel cell DC bus (1 V for diode losses).

| | 2S battery pack configuration | |
|---|---|---|
| | Low value | High value |
| Batt. voltage (V) | 6 | 8.4 |
| FC current (A) | 70 | 15 |
| FC power (W) | 490 | 140 |

the proper operation conditions of the power plant as can be seen in Fig. 7 where the polarization curve is depicted. The 2S pack voltage range is 6–8.4 V defining the fuel cell operation zone when it is coupled to the bus. Table 2 summarizes the theoretical limiting values for the fuel cell states. In the upper voltage limit, when the battery is fully charged (8.4 V), if the fuel cell is switched to the DC bus the voltage at the entrance of the diode will be 9.4 V and the fuel cell will respond delivering 15 A or 140 W, according to its polarization curve (Fig. 7). The lower limit sets a high power demand for the fuel cell due to the lower bus voltage, resulting in 70 A or close to the maximum power demand 490 W. The diode power loss will vary from 15 to 70 W, considering a nominal voltage drop of 1 V.

An active power plant design is more flexible because voltages can be adapted due to use of electronic power converters. This means that more options are available for the design of the power plant, which is only restricted by the functioning limits of the devices. Increasing the rated voltage of the battery minimizes the energy losses because of the decrease in the current intensity, but if fuel cell and battery voltages are too different the power converter efficiency diminishes. The low voltage of the USV fuel cell posed a challenge for the selection of a power converter and a customized device was designed and built to improve the system performance. Fig. 6 depicts the result of the manufactured power converter compared with a compact aeronautic power converter.

The large size could be a handicap for an aerial application, but not for a marine one where sometimes additional weight is necessary to ensure the hull stability. In any case, the customized converter still has some margin for size reduction, increasing the signal frequency to decrease the coil size. Additionally, both power converters where tested with the same power load and the efficiency analysis revealed that the customized converter achieved a better performance (95%) than the compact device (88%) with a lower temperature of the envelope (less than 32 °C versus 89 °C for the compact converter), which is an important factor for the USV integration.

### 3.1. Fuel cell characterization

The polarization curve of the developed fuel cell has been obtained in a test bench with an electronic programmable load. Fig. 7 shows the experimental results after data filtering. Blue dots are the average voltage for the demanded current intensity, red dots show the expected power delivered. The experiment was limited to 80 A but the power curve still showed an increasing tendency.

Experimental data has been adjusted to the theoretical equation proposed by Frano Barbir [22], shown as Eq. (1). This equation gives the voltage value for a single cell ($V_{cell}$) as function of current density ($i$).

$$V_{cell} = E_{r,T,P} - \frac{R \cdot T}{\alpha \cdot F} \ln\left(\frac{i + i_{loss}}{i_0}\right) - \underbrace{\frac{R \cdot T}{n \cdot F} \ln\left(\frac{i_L}{i_L - i}\right)}_{neglected} - i \cdot R_i \quad (1)$$

From the proposed equation the gas transport losses term is neglected because this phenomenon is not relevant for the working range as can be shown in the power curve tendency. Eq. (2) shows the numerical values for the fit to the fuel cell experimental polarization curve. The equation includes a correction for cell voltage and current values to adjust to the expected value for the stack. $N_c$ is the number of cells and $S_a$ is the MEA active area; 15 and 200 cm$^2$, respectively.

$$V_{FC} = N_c \cdot \left[440.409 \times 10^{-3} - 75.984 \times 10^{-3} \ln\left(\frac{I_{FC}}{S_a} + 2.026 \times 10^{-3}\right) - 124.910 \times 10^{-3} \cdot \frac{I_{FC}}{S_a}\right] \quad (2)$$

**Table 3**
Battery packs test results.

| Discharge rate | Maximum energy | Specific energy | Average power | Time (min) |
|---|---|---|---|---|
| 2S-battery pack (rated 170 W h or 191 W h kg$^{-1}$) | | | | |
| 05$C$ | 157 W h | 176 W h kg$^{-1}$ | 88 W | 107 min |
| 2$C$ | 144 W h | 161 W h kg$^{-1}$ | 338 W | 26 min |
| $P_{const}$ | 143 W h | 110 W h kg$^{-1}$ | 139 W | 63 min |
| 3S-battery pack (rated 255 W h or 193 W h kg$^{-1}$) | | | | |
| 05$C$ | 248 W h | 188 W h kg$^{-1}$ | 131 W | 113 min |
| 2$C$ | 240 W h | 182 W h kg$^{-1}$ | 510 W | 43 min |
| $P_{const}$ | 247 W h | 187 W h kg$^{-1}$ | 141 W | 108 min |

### 3.2. Battery characterization

The battery characterization was performed using a specialized battery tester from Arbin Instruments manufacturer (model: BT-ML 2016). The battery characterization only examined the battery discharge behavior, because the simulations and tests aimed to evaluate the USV range (maximum sailed distance). Both power plant energy reservoirs, the hydrogen tank and the batteries, were consumed during the tests.

The experimental procedure starts charging the battery at constant current until it reaches the maximum voltage and it remains stable, namely 8.4 V and 12.6 V for the 2S- and 3S-battery packs respectively. The discharge is performed at constant current until the battery pack voltage equals the minimum value considered, which is 6 V and 9 V for the 2S- and the 3S-battery, respectively. Battery pack temperature was monitored in each experiment as a security observer for the battery degradation. Only the 2C test for the 3S-battery pack reached to the maximum temperature but the test continued until the full discharge. Measured internal resistance for 2S-battery pack is 1.22 mΩ (0.61 mΩ per cell) and 1.70 mΩ (0.57 mΩ per cell) for the 3S-battery pack.

Fig. 8 depicts the battery tests, performed at ambient temperature. The two upper charts (Figs. 8(a) and 8(b)) show the experimental results for the 2S-battery pack (energy and temperature). The other two are for the 3S-battery pack test. Figs. 8(a) and 8(c) depict the energy extracted from the two battery packs with three different operation conditions. The green solid line is for the constant current discharge set as 05$C$ rate, which corresponds to ca. 11 A. The blue curve is also for constant current but with a high discharging rate of 2$C$, ca. 46 A. The red line, is for a controlled power discharge, using a USV power demand. It is the same power load that has been used for the power plant simulations and experimental validation, described in Sections 4 and 5, respectively. Figs. 8(b) and 8(d) show the battery pack temperature variation during the tests.

Table 3 summarizes the battery tests results. Rated energy per pack is 170 W h and 255 W h, at the minimal discharging rate, which means that the energy available suffers reduction of 8% and a 3% for the 2S- and the 3S-battery packs, respectively. This difference can also be due to the reduction of the internal resistance per cell for each battery pack. The power loss is increasing linearly with current. At the highest discharging rates the energy loss achieves a 15% and a 6% for the 2S- and 3S-battery, respectively, which is almost two-fold the 05$C$ discharging losses. Constant power discharge is very similar to 05$C$ due to the similarity in the average discharging power.

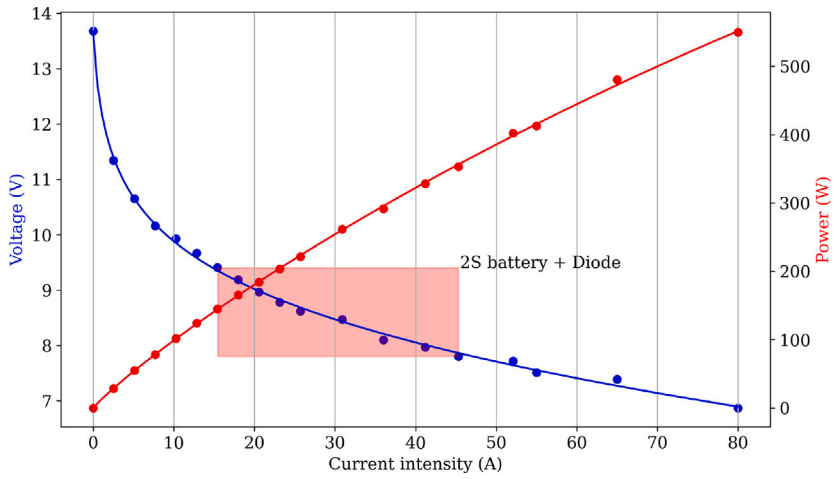


**Fig. 7.** Fuel cell polarization curve and 2S-battery pack voltage zone (after diode). (For interpretation of the references to color in this figure legend, the reader is referred to the web version of this article.)

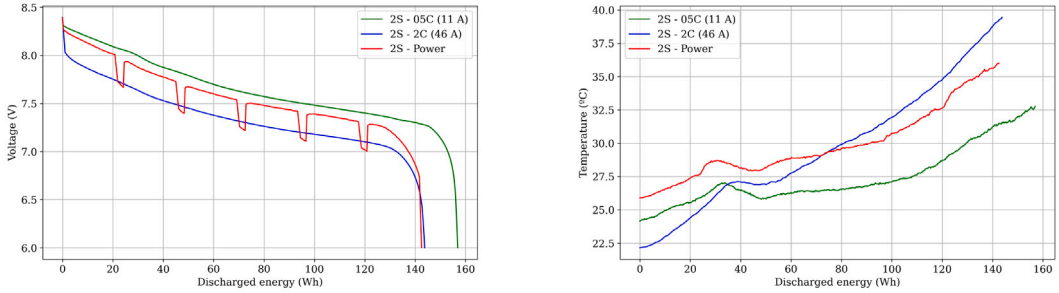


(a) Discharge test – 2S batt. pack (b) Temperature – 2S batt. pack

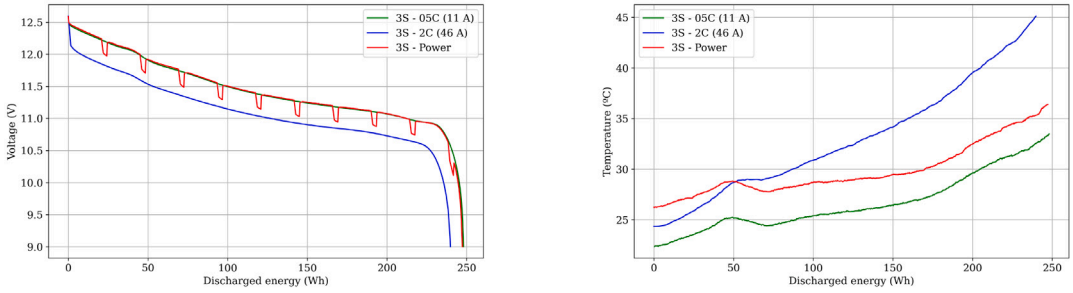


(c) Discharge test – 3S batt. pack (d) Temperature – 3S batt. pack

**Fig. 8.** Battery packs characterization, discharging test (constant power and current test). (For interpretation of the references to color in this figure legend, the reader is referred to the web version of this article.)

## 4. Hybrid power plant simulations

The methodology used for modeling and simulation of the physical systems is based on *Open Modelica*, which is a modeling software for mathematical representation of physical systems using differential and algebraic equations. This language provides an intuitive syntax for defining variables, parameters, and equations that describe the behavior of system components. Models are constructed using a combination of algebraic equations to represent static relationships and differential equations to describe the dynamic behavior of the system. It is a highly flexible environment that allows the representation of complex systems with multiple domains. Models can be built in a modular fashion, using not only predefined standard components but also creating customized components. This reusability of models and components accelerates the modeling process and facilitates collaboration across different projects. One of the primary strengths of Open Modelica is its capability to validate and optimize models before real implementation. Simulations performed with Open Modelica enable the evaluation of system behavior under various conditions and scenarios. This aids in identifying potential issues, such as instabilities or inefficiencies, and allows for design adjustments to optimize system performance. Additionally, Open Modelica provides advanced analysis tools, such as parameter identification and model optimization, further facilitating the improvement and refinement of the proposed models.

The use of Modelica language offers the ability to integrate the developed models with other systems and tools through standards like ROS (Robot Operating System) with simple languages. This allows for the coupling of simulation modules developed in Open Modelica with real-time control systems and leverages the functionalities provided

by ROS, such as inter-component communication and coordination of complex systems. This integration facilitates practical implementation and control of physical systems based on models developed with Open Modelica, what is commonly known as a Digital Twin.

### 4.1. Simulation results

The simulation performed aims to compare the physical behavior of four power plant configurations, namely, two active and two passive architectures. The objective of the simulation is not to define the real behavior but to analyze the expected performance of each power plant with a non-optimized power control algorithm. All four power plants are based on the functioning principle that the battery is the prime mover and the fuel cell acts as a range extender provider. In the case of the passive coupling a power switch controls the power delivery from the fuel cell. For the active architecture a DC-converter was set to control the power drain from the fuel cell.

The control algorithm for the switch or the DC-converter is also different for each configuration but all of them are defined to maintain the same battery levels: the fuel cell is connected when the minimum voltage of 3.3 V per cell is reached (corresponding to ≈ 25% of the state of charge, SoC), and turned off when the maximum voltage is achieved (4.2 V per cell). The four power plants configured for the simulations are named and described as follows:

**Passive 2S-batt.** Passive architecture power plant with a battery pack of two cells in series (2S). The power switch controls the connection of the fuel cell between the limits of 6.6 and 8.4 V.

**Passive 2S2P-batt.** Passive architecture power plant with a double battery pack of two cells in series (2S2P) connected in parallel. The power switch controls the connection of the fuel cell between the limits of 6.6 and 8.4 V. The purpose of this power plant configuration is to improve the range time for the previous passive configuration.

**Active 2S-batt.** Active architecture power plant with a battery pack of two cells in series (2S). The DC-converter activation is controlled by the battery pack voltage, in a range between 6.6 and 8.4 V.

**Active 3S-batt.** Active architecture power plant with a battery pack of three cells in series (3S). The control voltage levels are now 9.9 V and 12.6 V. The selection of the number of LiPo cells in series corresponds to the maximum voltage of the USV motor.

The simulation results are described and discussed in the next sections. Power curves (Section 4.1.1), current variations (4.1.2), voltage (4.1.3) and energy consumption (or state of charge) curves (4.1.4) are depicted and discussed.

The sign convention for the simulation results is based on the known "selfish" criterium. The current sign is defined as positive for a device if it enters the element, and negative if it is being "lost", i.e., the fuel cell always acts as a generator so it will always show a negative current. Batteries can gain or lose current. When the battery is being charged, current is gained, and the sign is positive. Negative current means a discharging situation. All the figures keep the same $x$-axis limit to help the time range comparative.

#### 4.1.1. Power curves

Fig. 9 shows the power variation for all the simulations. The curve color code is the same for all four graphs. The power load or demand is the blue line. The power load is defined as a USV working in a circuit or a loop with a constant demanded power, 125 W for 10 min and a peak demand for the ship manoeuvrability, when more power is required to change the ship direction. The peak demand was configured as a ramp increase of 5 s up to 400 W where it remains constant for 10 s and diminishing with the same rate. The power demand is always positive because it is absorbed by the load. The red curve is for the fuel cell power and the green line for the battery pack.

The graphs in Fig. 9 are for the four performed simulations. The top two correspond to the passive architecture and the bottom ones to the active configuration. The $x$-axis shows the time in hours. The end of each simulation is reached when no energy is available in the USV power plant, neither in hydrogen nor in battery.

During the periods where the battery and the fuel cell work together, it can be observed that the high power demand instants are supplied mainly by the battery energy. This means that the battery has a faster dynamic response, which is its main desirable characteristic for the hybridization. During these periods the battery is charged and when a power peak occurs it is supplied mainly by the battery, that stops absorbing power to release it, supplying the demanded power. The fuel cell increases gently the power, due to the voltage instability.

The fuel cell power demanded for the passive architectures is greater than that for the active power plants, because of the current control provided by the DC-converter. Abrupt changes in the fuel cell demanded power is one of its main degradation mechanisms. This seems to be more significant in the passive configurations where the demanded power gradient is greater that 400 W, and it is even worse when the battery capacity is lower, because more fuel cell contributions are required.

#### 4.1.2. Current intensity curves

Current curves are depicted in Fig. 10, organized in the same way and with the same color code as in the previous figure. The current in each case is defined by the power and the voltage. The load current is variable because the voltage is set by the battery, which depends on its capacity.

The high speed current variations are absorbed by the battery, due to its faster dynamics. In the passive configurations, fuel cell connections demand a very high current, and this can contribute to an early degradation. This problem can be mitigated changing the coupling and configuring the fuel cell as the prime mover (diode in the battery). This will avoid the degradation problem but at the expense of decreasing the vehicle range [14].

Some simple control issues can be observed. Fuel cell passive power plants decrease the delivered power when increasing the voltage of the battery pack, decreasing the supplied current. Active power plants show the opposite behavior: fuel cell current increases, as well as the battery absorbed current. This is because the DC-converter control algorithm sets a constant current injection to keep a constant power of 160 W, which means 15 A and 22 A, for the 2S- and 3S-battery packs, respectively. The USV integrated power plant control will include a state of health battery observer, to prevent overload during charging periods.

#### 4.1.3. Voltage curves

The voltage curves are smoother that the current and power ones. This is shown in the graphs of Fig. 11. The voltage for the load and the battery is the same (DC-bus voltage) so only the load is shown. Fuel cell voltage varies from the open circuit voltage (OCV) to the operation voltage. When there is no hydrogen available at the system, the fuel cell voltage goes to zero. Battery voltage varies from the minimum to the maximum per cell. Limits for the 2S-battery pack range from 6 to 8.4 V, and from 9 to 12.6 V for the 3S pack. The 2S2P-battery pack is like a 2S pack with augmented capacity.

In the passive power plants, fuel cell voltage follows the battery voltage plus the diode voltage drop. Diode voltage drop is what causes the power loss in passive architectures. In the active power plants, fuel cell voltage is the one that results from the power balance. When de DC-converter is switched, a constant output current is set as the reference control value. This reference current is set to release a 30% of extra power over constant the power demand.

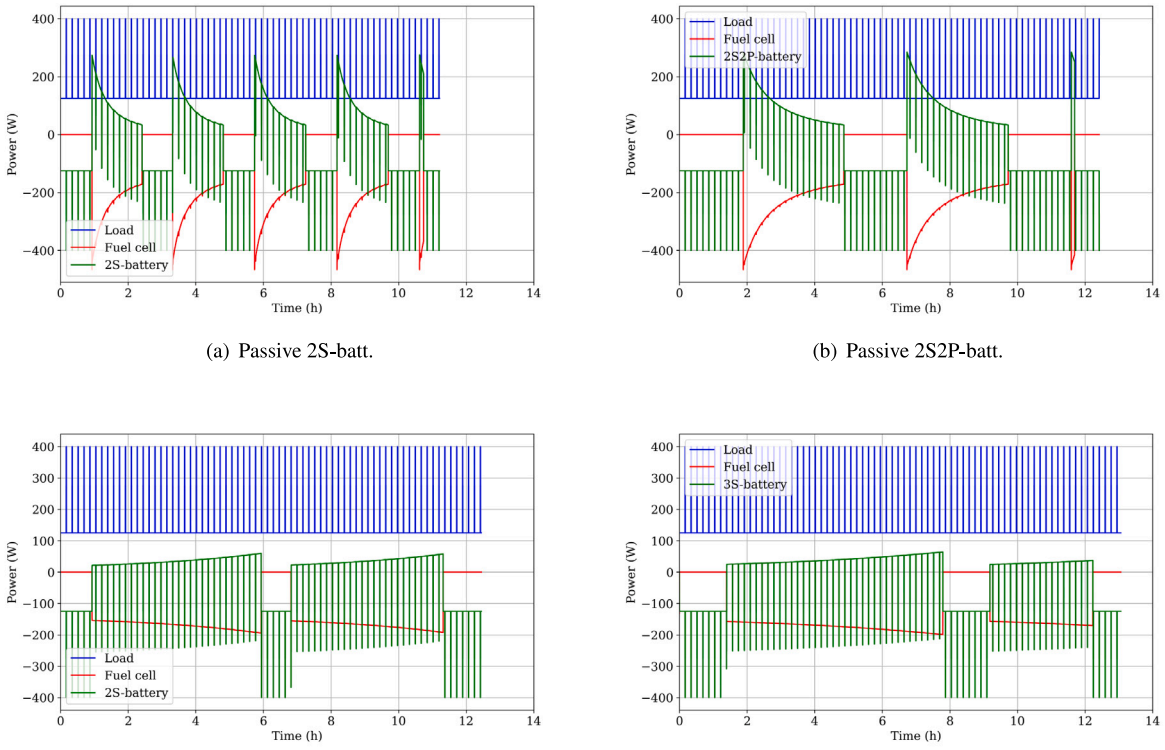


(a) Passive 2S-batt. (b) Passive 2S2P-batt.

(c) Active 2S-batt. (d) Active 3S-batt.

**Fig. 9.** Resulting power curves for the four simulations. (For interpretation of the references to color in this figure legend, the reader is referred to the web version of this article.)

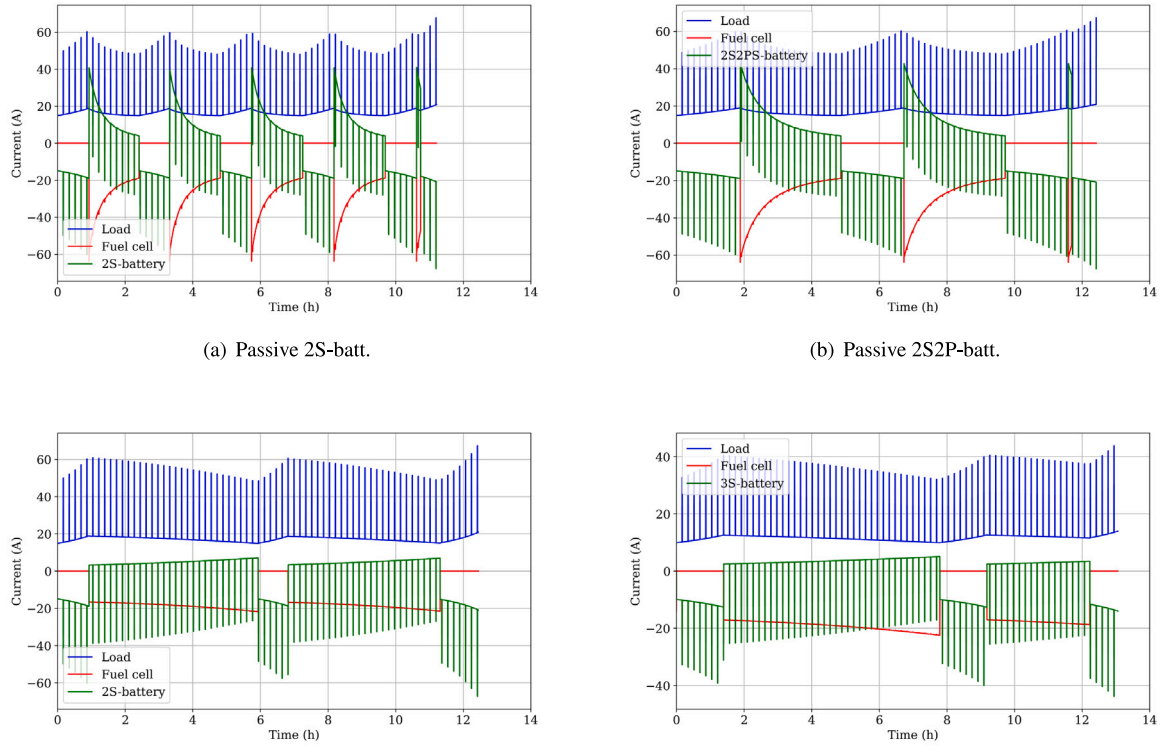


(a) Passive 2S-batt. (b) Passive 2S2P-batt.

(c) Active 2S-batt. (d) Active 3S-batt.

**Fig. 10.** Resulting current intensity curves for the four simulations. (For interpretation of the references to color in this figure legend, the reader is referred to the web version of this article.)

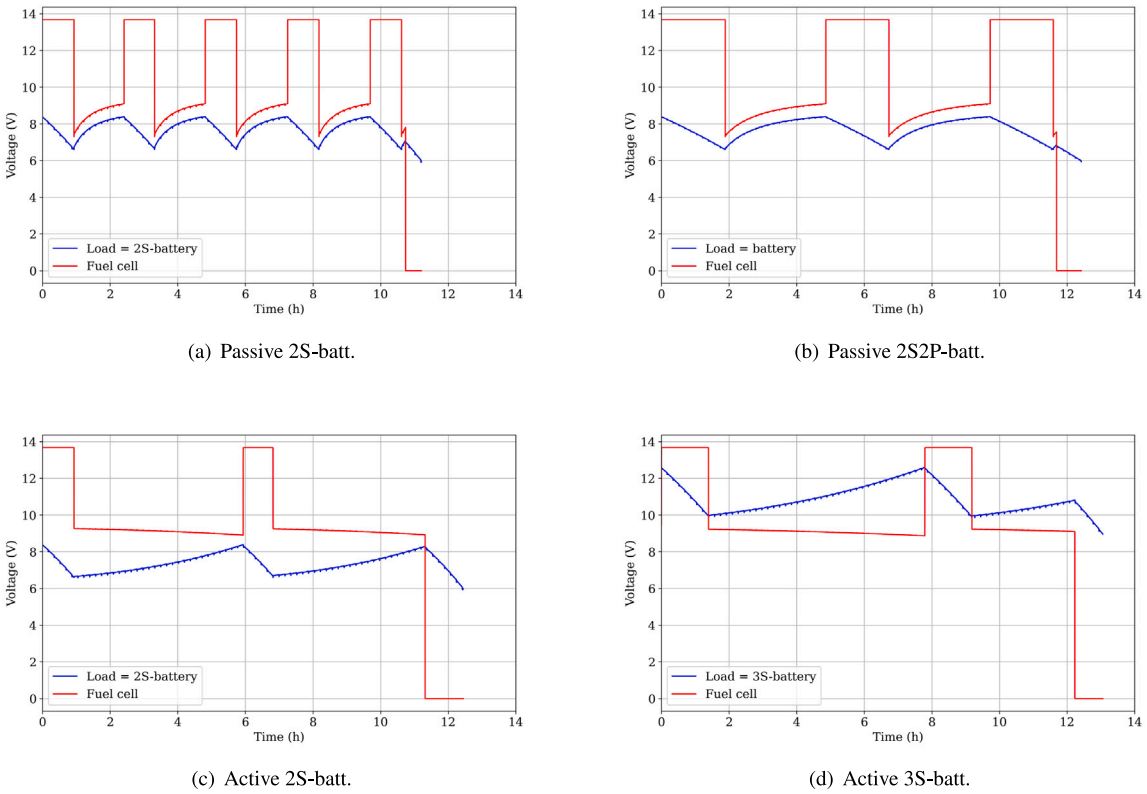


(a) Passive 2S-batt. (b) Passive 2S2P-batt.

(c) Active 2S-batt. (d) Active 3S-batt.

**Fig. 11.** Resulting voltage curves for the four simulations.

#### 4.1.4. Energy consumption curves

Graphs from Fig. 12 show the variation in the energy content of the power plant. Green lines correspond to the state of charge (SoC) of the battery pack, and red lines to the remaining load of the hydrogen storage system. Both lines are expressed in percentage of the maximum. Hydrogen capacity was estimated around 100 g. Maximum battery capacity depends on the number of cells in the pack.

The control system keeps the battery SoC inside the selected range. The different simulations show a different number of cycles for both, the battery and the fuel cell. Battery degradation is also affected by the number of cycles. The passive architecture with the smaller battery shows the worst behavior with the maximum number of charging-discharging battery cycles (Fig. 12(a)).

Battery charge rates are near 1$C$ for the active architecture power plant and starts near 2$C$ for the passive one, in this case with a decreasing rate. Ensuring a proper ventilation of the battery packs will maintain the temperature below the maximum admitted value.

Fig. 13 shows the specific power at the left and the rate of power lost over the power load. Attending to the specific energy criteria, the passive power plant with a double 2S-battery pack should be selected because it has the best energy ratio, 21% over the better active power plant. Nevertheless, the best use of hydrogen is achieved with the two active power plants, with a 8.5% improvement in hydrogen consumption, but with a huge penalty in total mass due to the DC-converter.

The green line in Fig. 13 shows the relative power losses of each system. For the passive architectures this value is estimated as the energy loss in the diode over the energy demanded by the load. Active architecture losses are due to the DC-converter efficiency. The simulated model considered a 95% efficiency for both cases. Contrary to the expected situation, the energy loss for the passive plants was higher than that for the active ones. This is because the losses in both cases are function of the current intensity and the passive architectures showed a higher current flow.

**Table 4**
Simulation results and performance.

| Passive 2S-batt. | Passive 2S2P-batt. | Active 2S-batt. | Active 3S-batt. |
|---|---|---|---|
| 15.591 kg | 16.487 kg | 19.341 kg | 19.765 kg |
| 101.8 W h kg$^{-1}$ | 114.6 W h kg$^{-1}$ | 87.9 W h kg$^{-1}$ | 95.6 W h kg$^{-1}$ |

Finally, the 12 h endurance objective is achieved by three of the four proposals. Therefore, the most suitable power plant is the one that not only satisfies the time objective but also ensures the maximum lifetime for all the power plant components. These requirements are all achieved with the active fuel cell 3S-battery power plant, which endures 13.4 h or around 37 km. This power plant not only shows the best performance, but also has the greatest potential for improvement due to its manageability. Specific energy has being determined weighting the main components of the power plant with the estimated mass values shown in Table 4.

## 5. Active hybrid power plant performance

Fig. 14(a) shows the experimental setup in the laboratory test bench for the active power plant with the assembled fuel cell and the 3S-battery pack (Active 3S-batt.). Power demand was simulated with an electronic programmable dynamic load (Hash Power: EAEL9080170B). Control and data logging were assembled in an electronic control board prototype (Fig. 14(b)), developed for the design and validation of the control strategy and the energy management system before the USV integration. The final control board will also be based in Arduino architecture but with an integrated and compact design. The experimental validation was focused in assessing the accuracy of the power plant model. This is why tests extended only for 4 h.

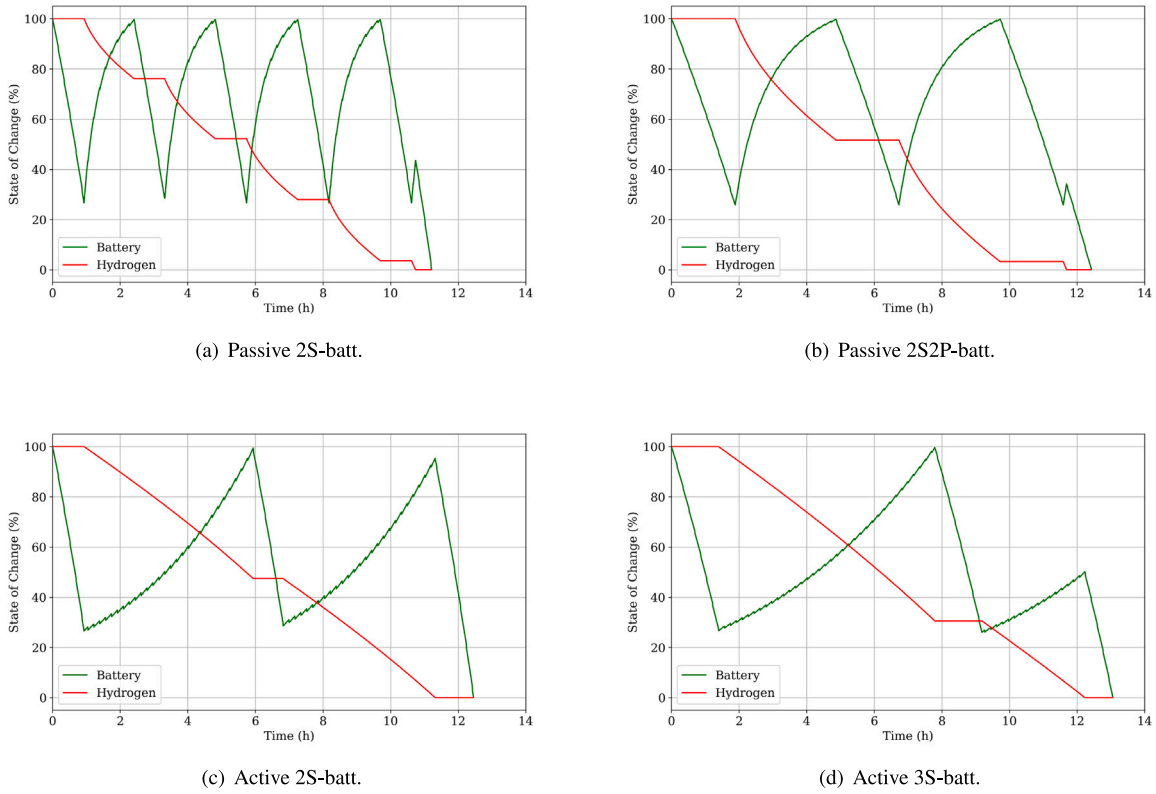


(a) Passive 2S-batt. (b) Passive 2S2P-batt.

(c) Active 2S-batt. (d) Active 3S-batt.

**Fig. 12.** Comparation of the SoC variation. (For interpretation of the references to color in this figure legend, the reader is referred to the web version of this article.)

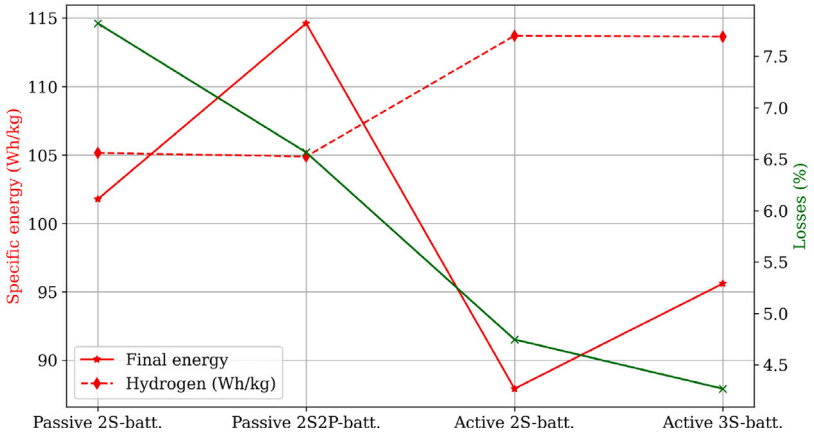


**Fig. 13.** Simulation results: specific energy and power losses. (For interpretation of the references to color in this figure legend, the reader is referred to the web version of this article.)

### *5.1. Power plant control for testing procedure*

The control algorithm of hybrid fuel cell-battery power plants is a key point for the design of a successful unmanned vehicle. The development of the control algorithm is out of the scope of this work, but the right sizing and selection of the components is affected by it. The diagram of Fig. 15 shows not only the electrical connections but also some sensoring and control signals required for plant control. The USV control system will be developed in two levels. On the one hand, a high level control algorithm based on Robotic Operational System (ROS) and an embedded computer with navigation and high information processing capabilities. On the other hand a low level control algorithm in a customized Arduino-based electronic board. High level control is in charge of the vehicle navigation and decision-making according to the energy level and power plant state, that the low level control system communicates to the ROS system by the USB protocol developed for this purpose.

Low level control system does not mean a simple system. On the contrary, it is the first front control system, simple enough to keep the power system alive and ensuring the USV return to the ground control station or the base in case of navigation failure. The proposed low level control for the present performance analysis is a state-machine based on a battery capacity (SoC) observer, using the fuel cell for a range extension. This simple strategy has been developed by other authors as a starting point [16,23]

Nevertheless, the low level control architecture is able to integrate predictive control algorithms thanks to the new low processing demand machine learning libraries for Arduino [24]. Existent works have shown that simple control systems for the use of batteries-fuel cell hybridization minimize fuel cell ageing and degradation [23].

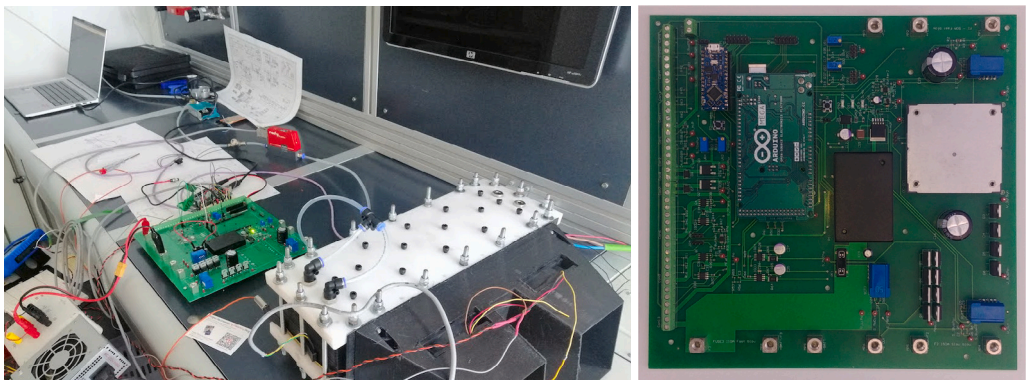

(a) Power plant test inside the USV (b) Customized electronic control test board

**Fig. 14.** Experimental setup for the hybrid power plant test.

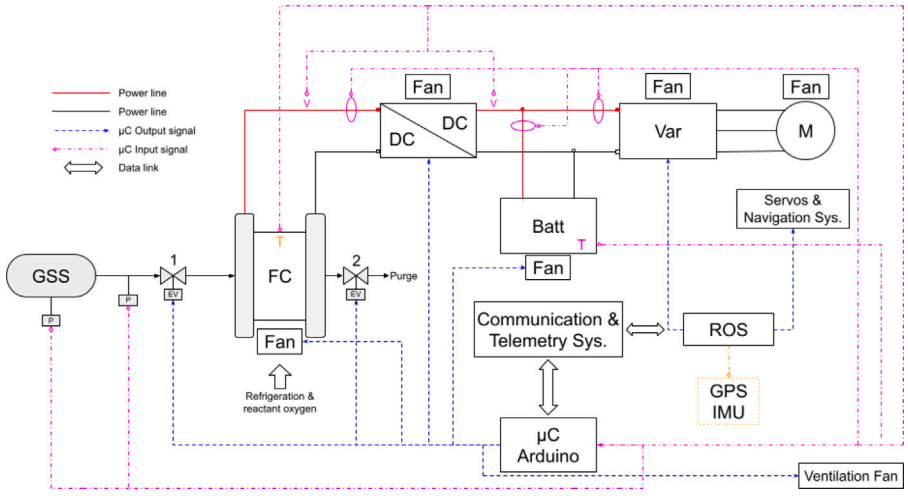


**Fig. 15.** Power plant power configuration diagram.

Furthermore, inclusion of ultracapacitors in combination with batteries and fuel cells improve the power plant for the very high dynamic power transients in unpredictable environments [23,25,26]. Fuzzy control is proposed as a good algorithm to keep the fuel cell operation in the best efficiency point while monitoring the state of health of all the energy sources [17,27].

### 5.2. Power plant test bench performance

Experimental results are shown in Fig. 16, where blue color lines correspond to the load parameters, green lines stand for the battery and red ones for the hydrogen fuel cell. Magenta color is for the DC-converter output parameters, namely, current and power. Simulation results (Section 4) are overlapped with experimental data, using dashed lines with the same color coding. Experimental and simulated power load matches perfectly because it is a mathematical expression (Fig. 16(c)). The small differences are due to signal measurement errors in the experimental data. The identified differences will be explained below.

Fig. 16(a) depicts the voltage curves. Blue line is for the DC bus, which includes the battery, load and DC-converter output. Both blue lines show a very good agreement between the simulation and the experimental results. Simulated and experimental voltages are parallel and with similar slope because only the battery affects them. The voltage difference between them is caused by the real resistance of the wires and electrical elements, which was not considered in the simulation. This can be also deduced from the current chart (Fig. 16(b)), where the experimental current is always higher to meet the same demanded load because of a lower voltage.

It can be observed that there is a delay in the simulation an experimental first connection of the fuel cell. The reason for that is because the control algorithm was programmed with a voltage measurement hysteresis to ensure the right estimation of the battery SoC and avoid control flickering.

The current output from the power converter is the same for the experimental data and the simulation (magenta in Fig. 16(b)). It is set in the control algorithm. However, the fuel cell current is different in both situations. The difference in fuel cell operation point is due to the DC-converter efficiency. For the simulation the considered efficiency was 95% but the experimental measured efficiency is 86.2%, ca. 9% lower than the obtained with the DC-converter test. This can be due to some degradation after all the tests performed to the customized DC-converter.

The state of charge for the energy storage system is shown in Fig. 16(d). The red line shows the hydrogen content in the pressurized bottle. The green lines depict the battery remaining capacity over the nominal one. Experimental curves are numerically estimated integrating the delivered energy from both the battery and the fuel cell. During the first period (without fuel cell) the real consumption rate matches the simulation rate with a small difference due to the real resistance. When the fuel cell starts, the consumption rates appear very different. Considering the data from the experiments and the simulations, the plant efficiencies are estimated in 95.7% and 89.1%, respectively. This means that the real power plant is able to achieve an endurance of ca. 12.5 h, nearly an hour less than the simulation endurance.

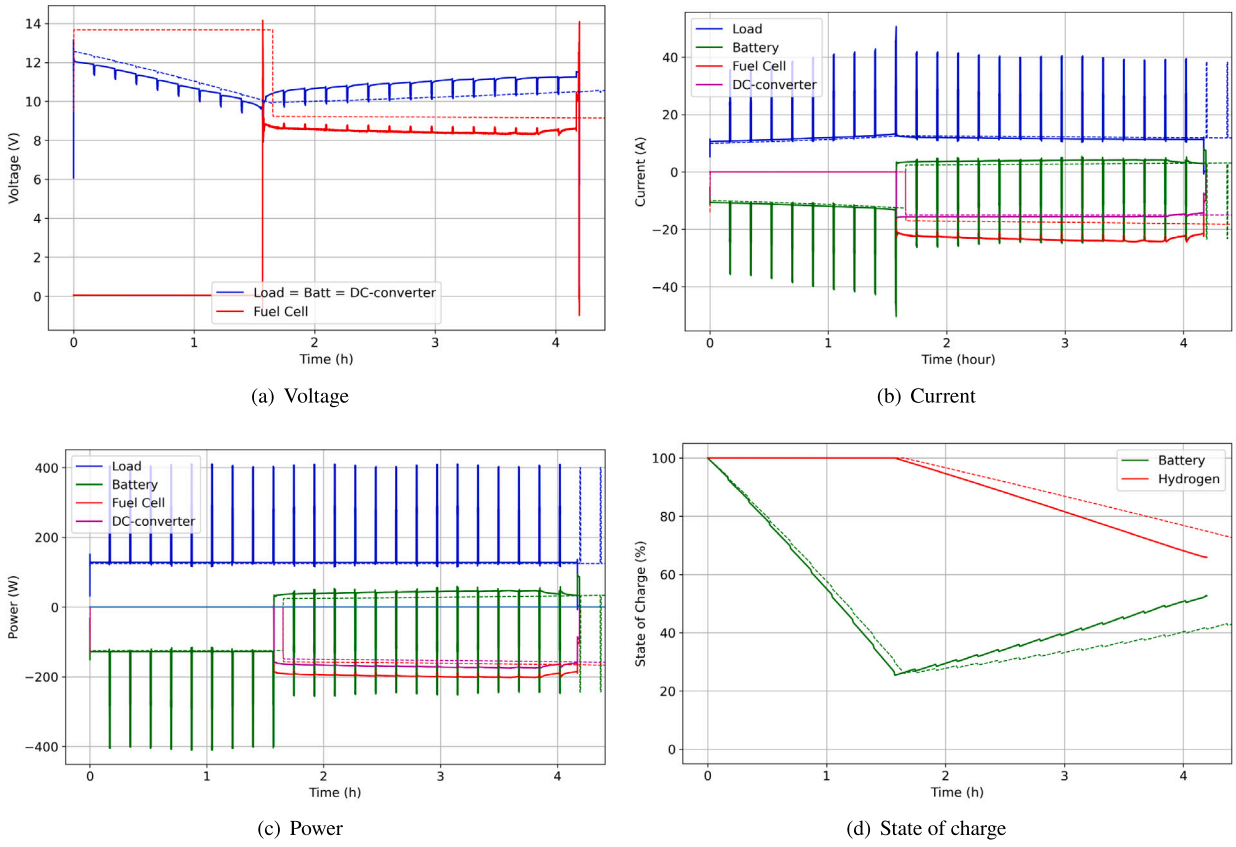


(a) Voltage (b) Current

(c) Power (d) State of charge

**Fig. 16.** Experimental results for active power plant architecture. (For interpretation of the references to color in this figure legend, the reader is referred to the web version of this article.)

Finally, it should be noted that there is a difference between the fuel cell idle voltage in the experiment (0 V) and the simulation (≈14 V) (Fig. 16(a)). It is caused by the control system algorithm, and it does not change any of the results. The simulation assumes that the fuel cell is always flooded with hydrogen and the fuel cell idles in the open circuit voltage. The real control algorithm supplies hydrogen when power is demanded to the fuel cell. The main reason for this difference is that the simulation is simpler and the real power plant is safer, as it avoids hydrogen leakages and accumulation.

## 6. Conclusions and future work

Hybridization of fuel cell power plants is necessary to improve the fuel cell performance, stabilizing the operation point, minimizing the power demanded to it and extending its lifetime. All the performed analysis, namely simulations and experimental tests, show that large power variations are absorbed by the battery pack while the fuel cell power remains constant thanks to the DC-converter control. The good simulation results encourage us to improve the USV modellization to include the hydrodynamic behavior in order to develop a vehicle digital twin that could be integrated into the navigation system (ROS) to solve a decision-making optimization algorithm to improve the energy efficiency of the system. The study has shown that a simple control algorithm is able to extend the navigation more that 12 h in calm waters. This means that an optimized energy management system should be able to extend the range with the same energy content that achieves a specific value of $85.6\,\mathrm{W\,h\,kg^{-1}}$

## Declaration of competing interest

The authors declare that they have no known competing financial interests or personal relationships that could have appeared to influence the work reported in this paper.

## Acknowledgments

This work has been entirely funded by the Spanish Ministry of Science, Innovation and Universities under the project DOVELAR (Ref.: RTI2018-096001-B-C33).

## References

[1] Sanguesa Julio A, Torres-Sanz Vicente, Garrido Piedad, Martinez Francisco J, Marquez-Barja Johann M. A review on electric vehicles: Technologies and challenges. Smart Cities 2021-03-15;4(1):372–404. http://dx.doi.org/10.3390/smartcities4010022, URL https://www.mdpi.com/2624-6511/4/1/22.

[2] Bernard Jérôme, Hofer Marcel, Hannesen Uwe, Toth Antoine, Tsukada Akinori, Büchi Félix N, Dietrich Philipp. Fuel cell/battery passive hybrid power source for electric powertrains. J Power Sources 2011-07;196(14):5867–72. http://dx.doi.org/10.1016/j.jpowsour.2011.03.015, URL https://linkinghub.elsevier.com/retrieve/pii/S0378775311005970.

[3] Sohn Seok-In, Oh Jung-Hwan, Lee Yeon-Seung, Park Dae-Hwan, Oh Il-Kwon. Design of a Fuel-Cell-Powered Catamaran-Type Unmanned Surface Vehicle. IEEE J Ocean Eng 2015-04;40(2):388–96. http://dx.doi.org/10.1109/JOE.2014.2315889, ISSN 0364-9059, 1558-1691, 2373-7786. URL http://ieeexplore.ieee.org/document/6818449/.

[4] Zhang Xiaohui, Liu Li, Dai Yueling, Lu Tianhe. Experimental investigation on the online fuzzy energy management of hybrid fuel cell/battery power system for UAVs. Int J Hydrogen Energy 2018-05;43(21):10094–103. http://dx.doi.org/10.1016/j.ijhydene.2018.04.075, URL https://linkinghub.elsevier.com/retrieve/pii/S036031991831200X.

[5] Roda Vicente, Carroquino Javier, Valiño Luis, Lozano Antonio, Barreras Félix. Remodeling of a commercial plug-in battery electric vehicle to a hybrid configuration with a PEM fuel cell. Int J Hydrogen Energy 2018-08;43(35):16959–70. http://dx.doi.org/10.1016/j.ijhydene.2017.12.171, URL https://linkinghub.elsevier.com/retrieve/pii/S0360319917348929.

[6] Chen Yong-Song, Lin Sheng-Miao, Hong Boe-Shong. Experimental study on a Passive Fuel Cell/Battery Hybrid Power System. Energies 2013-12-10;6(12):6413–22. http://dx.doi.org/10.3390/en6126413, URL http://www.mdpi.com/1996-1073/6/12/6413.

[7] López González Eduardo, Sáenz Cuesta Jaime, Vivas Fernandez Francisco J, Isorna Llerena Fernando, Ridao Carlini Miguel A, Bordons Carlos, Hernandez Emili, Elfes Alberto. Experimental evaluation of a passive fuel cell/battery hybrid power system for an unmanned ground vehicle. Int J Hydrogen Energy 2019-05;44(25):12772–82. http://dx.doi.org/10.1016/j.ijhydene.2018.10.107, URL https://linkinghub.elsevier.com/retrieve/pii/S0360319918333068.

[8] Thangavelautham Jekanthan, Gallardo Danielle, Strawser Daniel, Dubowsky Steven. Hybrid fuel cell power for long duration robot missions in field environments. In: Field robotics. WORLD SCIENTIFIC; 2011-08, p. 471–8. http://dx.doi.org/10.1142/9789814374286_0055, ISBN 978-981-4374-27-9 978-981-4374-28-6. URL http://www.worldscientific.com/doi/abs/10.1142/9789814374286_0055.

[9] Hwang Jenn Jiang, Chang Wei Ru. Characteristic study on fuel cell/battery hybrid power system on a light electric vehicle. J Power Sources 2012-06;207:111–9. http://dx.doi.org/10.1016/j.jpowsour.2012.02.008, URL https://linkinghub.elsevier.com/retrieve/pii/S0378775312003096.

[10] Fathabadi Hassan. Combining a proton exchange membrane fuel cell (PEMFC) stack with a Li-ion battery to supply the power needs of a hybrid electric vehicle. Renew Energy 2019-01;130:714–24. http://dx.doi.org/10.1016/j.renene.2018.06.104, URL https://linkinghub.elsevier.com/retrieve/pii/S0960148118307560.

[11] De Lorenzo Giuseppe, Piraino Francesco, Longo Francesco, Tinè Giovanni, Boscaino Valeria, Panzavecchia Nicola, Caccia Massimo, Fragiacomo Petronilla. Modelling and performance analysis of an autonomous marine vehicle powered by a fuel cell hybrid powertrain. Energies 2022-09-21;15(19):6926. http://dx.doi.org/10.3390/en15196926, URL https://www.mdpi.com/1996-1073/15/19/6926.

[12] Bendjedia Bachir, Rizoug Nassim, Boukhnifer Moussa, Bouchafaa Farid, Benbouzid Mohamed. Influence of secondary source technologies and energy management strategies on Energy Storage System sizing for fuel cell electric vehicles. Int J Hydrogen Energy 2018-06-21;43(25):11614–28. http://dx.doi.org/10.1016/j.ijhydene.2017.03.166, URL https://www.sciencedirect.com/science/article/pii/S0360319917311722.

[13] Thomas CE. Fuel cell and battery electric vehicles compared. Int J Hydrogen Energy 2009-08-01;34(15):6005–20. http://dx.doi.org/10.1016/j.ijhydene.2009.06.003, URL https://www.sciencedirect.com/science/article/pii/S0360319909008696.

[14] Renau Jordi, Barroso Jorge, Sánchez Fernando, Martí n Jesús, Roda Vicente, Barreras Felix. Test performance of a fuel cell based power plant for a high altitude light unmanned aerial vehicle. Zaragoza 2016;2.

[15] Bai Xingying, Jian Qifei, Huang Bi, Luo Lizhong, Chen Yangyang. Hydrogen starvation mitigation strategies during the start-up of proton exchange membrane fuel cell stack. J Power Sources 2022-02-01;520:230809. http://dx.doi.org/10.1016/j.jpowsour.2021.230809, URL https://www.sciencedirect.com/science/article/pii/S0378775321013008.

[16] Chen Huicui, Zhao Xin, Zhang Tong, Pei Pucheng. The reactant starvation of the proton exchange membrane fuel cells for vehicular applications: A review. Energy Convers Manage 2019-02-15;182:282–98. http://dx.doi.org/10.1016/j.enconman.2018.12.049, URL https://www.sciencedirect.com/science/article/pii/S0196890418313852.

[17] Li Jianwei, Wang Hanxiao, He Hongwen, Wei Zhongbao, Yang Qingqing, Igic Petar. Battery optimal sizing under a synergistic framework with DQN-based power managements for the fuel cell hybrid powertrain. IEEE Trans Transp Electrif 2022-03;8(1):36–47. http://dx.doi.org/10.1109/TTE.2021.3074792.

[18] Zimmermann Thomas, Keil Peter, Hofmann Markus, Horsche Max F, Pichlmaier Simon, Jossen Andreas. Review of system topologies for hybrid electrical energy storage systems. J Energy Storage 2016-11;8:78–90. http://dx.doi.org/10.1016/j.est.2016.09.006, URL https://linkinghub.elsevier.com/retrieve/pii/S2352152X16301566.

[19] Samsun Remzi Can, Krupp Carsten, Baltzer Sidney, Gnörich Bruno, Peters Ralf, Stolten Detlef. A battery-fuel cell hybrid auxiliary power unit for trucks: Analysis of direct and indirect hybrid configurations. Energy Convers Manage 2016-11;127:312–23. http://dx.doi.org/10.1016/j.enconman.2016.09.025, URL https://linkinghub.elsevier.com/retrieve/pii/S0196890416308020.

[20] Andreasen S, Ashworth L, Menjonremon I, Kar S. Directly connected series coupled HTPEM fuel cell stacks to a Li-ion battery DC bus for a fuel cell electrical vehicle. Int J Hydrogen Energy 2008-12;33(23):7137–45. http://dx.doi.org/10.1016/j.ijhydene.2008.09.029, URL https://linkinghub.elsevier.com/retrieve/pii/S0360319908011452.

[21] Alegre Cinthia, Lozano Antonio, Manso Angel Perez, Alvarez-Manuel Laura, Marzo Florencio Fernandez, Barreras Felix. Single cell induced starvation in a high temperature proton exchange membrane fuel cell stack. Appl Energy 2019-09;250:1176–89. http://dx.doi.org/10.1016/j.apenergy.2019.05.061, URL https://linkinghub.elsevier.com/retrieve/pii/S0306261919309171.

[22] Barbir Frano. Fuel cell electrochemistry. In: PEM fuel cells. Elsevier; 2013, p. 33–72. http://dx.doi.org/10.1016/B978-0-12-387710-9.00003-5, URL https://linkinghub.elsevier.com/retrieve/pii/B9780123877109000035.

[23] Colnago Silvia, Mauri Marco, Piegari Luigi. Energy management strategy for a fuel cell/lead acid battery/ ultracapacitor hybrid electric vehicle. In: 2020 IEEE vehicle power and propulsion conference (VPPC). 2020-11, p. 1–5. http://dx.doi.org/10.1109/VPPC49601.2020.9330836.

[24] Warden Pete, Situnayake Daniel. TinyML: Machine learning with tensorflow lite on arduino and ultra-low-power microcontrollers. First edition. O'Reilly; 2020.

[25] Schaltz Erik, Khaligh Alireza, Rasmussen Peter Omand. Influence of battery/ultracapacitor energy-storage sizing on battery lifetime in a fuel cell hybrid electric vehicle. IEEE Trans Veh Technol 2009-10;58(8):3882–91. http://dx.doi.org/10.1109/TVT.2009.2027909.

[26] Bizon Nicu, Radut Marin, Oproescu Mihai. Energy control strategies for the fuel cell hybrid power source under unknown load profile. Energy 2015-06;86:31–41. http://dx.doi.org/10.1016/j.energy.2015.03.118, URL https://linkinghub.elsevier.com/retrieve/pii/S0360544215004673.

[27] Hu Xiao, Liu Shikun, Song Ke, Gao Yuan, Zhang Tong. Novel fuzzy control energy management strategy for fuel cell hybrid electric vehicles considering state of health. Energies 2021-01;14(20):6481. http://dx.doi.org/10.3390/en14206481, URL https://www.mdpi.com/1996-1073/14/20/6481.